AFRL-SR-AR-TR-03-

$O413$

' I 2003

REPORT DOCUMENTATION PAGE

1. REPORT DATE (DD-MM-YYYY) 07/31/2003	2. REPORT TYPE Final	3. DATES COVERED (From - To) April 2000 - April 2003

4. TITLE AND SUBTITLE

Hybrid Control of Jet Flows

5a. CONTRACT NUMBER

5b. GRANT NUMBER

F49620-00-1-0255

5c. PROGRAM ELEMENT NUMBER

6. AUTHOR(S)

Naughton, Jonathan, W
Smith, Douglas, R

5d. PROJECT NUMBER

5e. TASK NUMBER

3484/BS

5f. WORK UNIT NUMBER

7. PERFORMING ORGANIZATION NAME(S) AND ADDRESS(ES)

University of Wyoming
PO Box 3355
Laramie, WY 82071

8. PERFORMING ORGANIZATION REPORT NUMBER

UWAL-2003-01

9. SPONSORING/MONITORING AGENCY NAME(S) AND ADDRESS(ES)

Air Force Office of Scientific Research (AFOSR)
4015 Wilson Blvd., Arlington, VA 22203

10. SPONSOR/MONITOR'S ACRONYM(S)

11. SPONSOR/MONITOR'S ____

20031028 131

12. DISTRIBUTION/AVAILABILITY STATEMENT

Approval for public release; distribution is unlimited.

13. SUPPLEMENTARY NOTES

14. ABSTRACT

The use of swirl and synthetic jet actuators in a hybrid control scheme is described. The results here are limited to the characterization of (1) swirling jet flows and (2) synthetic jets in a two-dimensional mixing layer. Jets with swirl numbers of 0.10 and 0.23 with different tangential velocity profiles were studied. The lower swirl jets behaved similarly to non-swirling jets, whereas the higher swirl jets enhanced mixing significantly, up to 40% for the cases studied here. At the nozzle exit, higher turbulence levels were observed in the swirling jets, and the investigation of the effect of swirl on turbulent structure continues. Synthetic jet actuators on the trailing edge of a splitter plate were studied in two orientations - aligned spanwise to the flow and aligned with the flow. The actuator oriented spanwise to the flow enhanced the streamwise vortices in the mixing layer yielding an increase in non-dimensional mixing layer growth rate of 53%, whereas the other orientation produced little change in the streamwise vortices and only produced a 19% increase.

15. SUBJECT TERMS

Active control; passive control; hybrid control; swirling jets; actuators; mixing enhancement

16. SECURITY CLASSIFICATION OF:			17. LIMITATION OF ABSTRACT	18. NUMBER OF PAGES	19a. NAME OF RESPONSIBLE PERSON
a. REPORT	b. ABSTRACT	c. THIS PAGE	UU	28	Jonathan W. Naughton
U	U	U			19b. TELEPHONE NUMBER (Include area code) (307)766-6284

Hybrid Control of Jet Flows

J. W. Naughton and D. R. Smith

Report UWAL-2003-01

Department of Mechanical Engineering
University of Wyoming, Laramie, WY 82071

July 31, 2003

Introduction

The goal of this study was to demonstrate hybrid flow control – the combination of active and passive control methodologies to produce control authority greater than would be possible using either method alone. If a flow is first destabilized using passive means, then it is likely that active control methodologies will be more effective than in the same flow with no passive control. The flow field chosen for study here is the incompressible turbulent jet. The passive control to be used is swirl, and the active control is to be provided using synthetic jet actuators. Before attempting hybrid control, a thorough characterization of both the passive control (i.e. swirling jets) and active control (i.e. synthetic jets) methodologies was undertaken. The synthetic jets were studied in a two-dimensional mixing layer to produce a situation similar to that which would be experienced when introducing disturbances into the swirling jet.

At present, the individual flows are still being characterized, a task that required more time than anticipated. A description of the work carried out in these two flows is summarized in the following sections. It is anticipated that, in the near future, open-loop hybrid jet control will be demonstrated.

Swirling Jet Flows

An understanding of the mechanisms causing enhanced growth rates in swirling jet flows was the goal of this part of the study. As part of this work, a thorough documentation of the effect of initial swirl profile on jet growth rates using mean flow-field measurements has been completed. Single-point and two-point fluctuating flow field measurements followed the mean measurements and provided insight into the effects of swirl on turbulence and the mechanisms causing the changes in the turbulence. The fluctuating measurements are continuing at this time.

The swirling jet measurements have been carried out in a well conditioned flow free from artifacts of the swirl generation process. A list of test cases is provided in Table 1 where the individual cases have been listed by the type of swirl profile and the swirl number S given by

$$S = \frac{G_\theta}{RG_z} = \frac{\int_o^r 2\pi\rho r^2 \bar{u}\bar{w}\,dr}{R\int_o^r 2\pi\rho r \bar{u}^2\,dr},\tag{1}$$

where G_θ is the axial flux of angular momentum, G_z is the axial flux of axial momentum, R is the nozzle exit radius, r is the radial coordinate, ρ is the density, $\bar{u}$ is

Table 1: Test cases for the present study.

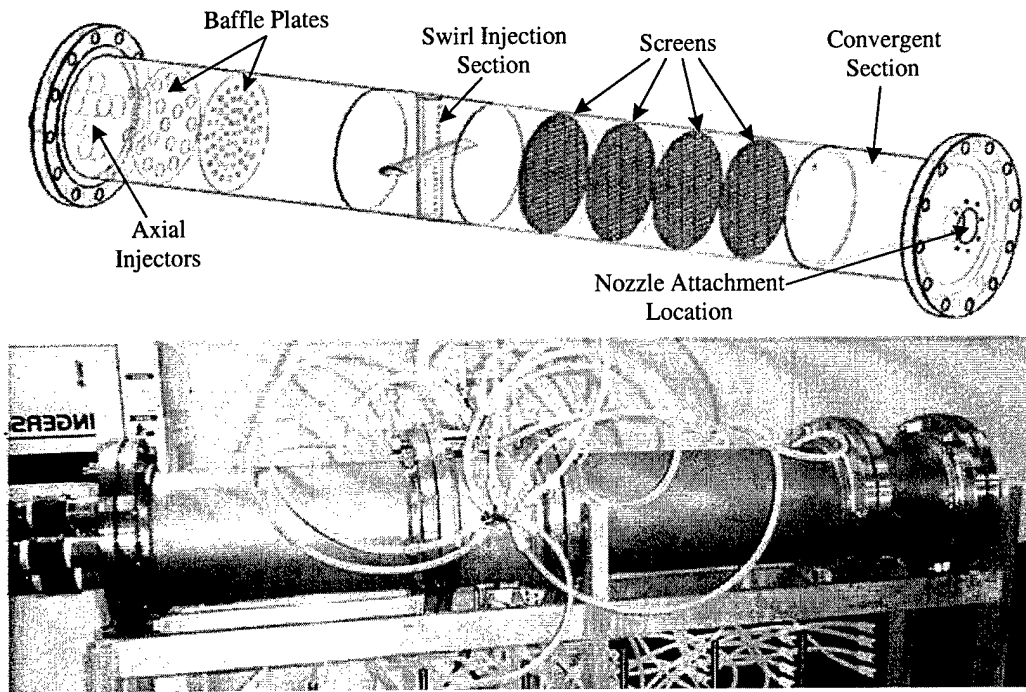| Case Number	Swirl Type	S
1	Non-Swirling	0.00
2	q-Vortex	0.10
3	q-Vortex	0.23
4	Solid Body	0.10
5	Solid Body	0.23

Figure 1: Swirling jet facility.

the mean axial velocity, and $\bar{w}$ is the mean tangential velocity. During testing, the flow was adjusted such that the average axial exit velocity was the same for all five cases. The Reynolds number based on average nozzle exit axial velocity and nozzle diameter was 1×10^5 for all cases.

Facility Development

A critical aspect of the work proposed here was the successful modification of a free jet facility to provide the capability of producing swirling jets with different tangential velocity profiles. An in-depth description of the facility can be found in reference [1], but a brief description is provided here. A picture of the completed facility can be seen in Fig. 1. The axial flow to the jet is supplied primarily by a regenerative blower. The air from the blower passes through two baffle plates and a honeycomb insert before entering the swirl injection insert. The flow passes through the swirl injection insert and four screens before entering a 11:1 contraction section. The flow leaving the contraction section enters a converging nozzle with a 4:1 inlet-to-exit area ratio and a 38.1 mm exit diameter. Using the current blower capacity, the free jet can provide velocities up to 70 m/s, which yields Reynolds numbers up to 1.33×10^5 based on nozzle exit diameter. The housing for the free jet is stainless pipe lined with PVC pipe so the facility can be easily upgraded to higher pressure for compressible flow work.

The swirl injection section is supplied by a separate compressed air supply. Air from a storage tank enters a manifold that supplies 8 regulators with high-pressure
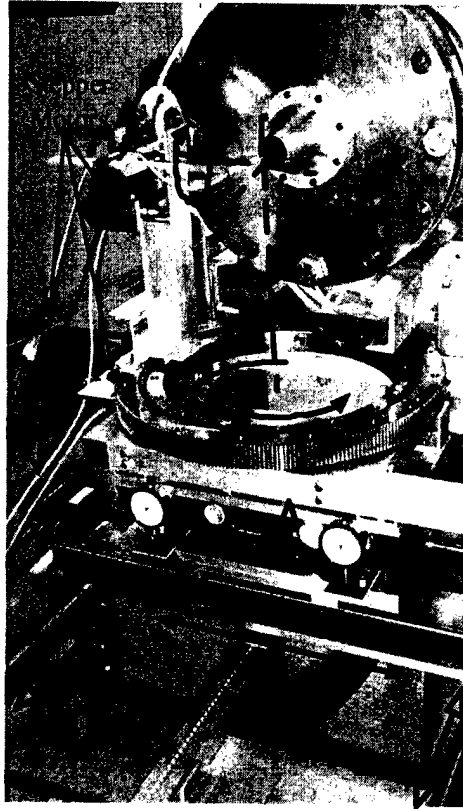
2

Figure 2: Traverse system developed for the swirling jet facility.

air (860 kPa). The regulators govern the pressure of the air injected through four injection ports located at the same distance from the stilling chamber axis. There are eight groups of four injectors located at different radii for a total of 32 injection ports. Unique to this facility is the flow conditioning that takes place downstream of the swirl injection section. Four screens and the large contraction ratio ensure that all artifacts of the swirl generation have been eliminated. Results indicate that, even with the flow conditioning, a wide range of swirl profiles may be produced using this system.

The development of a flexible traverse system was critical for acquiring the swirling jet data necessary for this study. The traverse, shown in Fig. 2, was designed to operate in two different modes: a calibration mode, and a jet-axis-centered mode. A schematic of the coordinate system associated with the jet flow field is shown in Fig. 3. In the calibration mode, the traverse has 5 axes of control: three translational (x, y, z) and two angular (pitch α and yaw β). A five-hole probe and several cross-wire probes have been automatically calibrated using this system. In the jet-axis-centered mode, the traverse may be used to rotate a rake of hot wires about the jet axis. In this mode, the traverse has two active axes of control: one translational (controls z location manually) and one angular (controls θ using a stepper motor). By leaving one probe
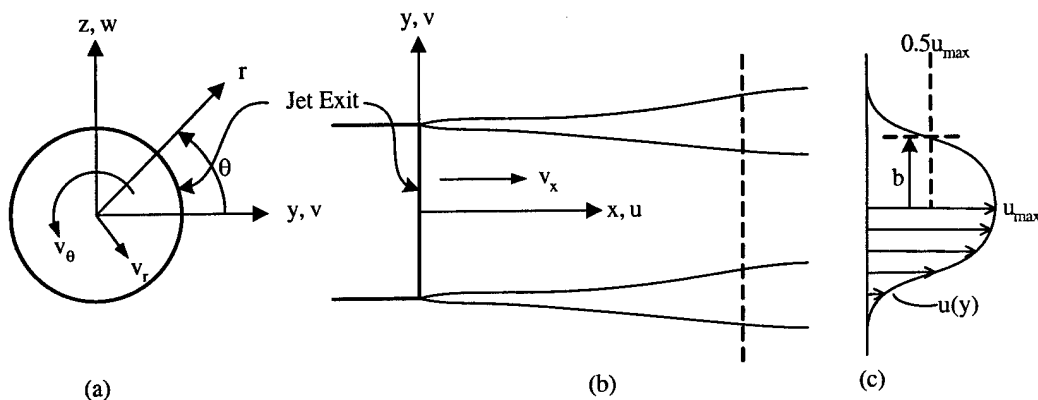
3

Figure 3: Schematic of swirling jet showing coordinate system and important parameters: (a) view looking from downstream toward the nozzle exit; (b) plan view; and (c) representation of the axial velocity profile along the dashed line in (b) for z=0.

stationary and moving a group of probes mounted to a strut, two-point correlations in a r-θ plane may be mapped out automatically. Such two-point correlations are currently being carried out using this system.

Mean Flow-Field Measurements

A brief summary of mean-flow measurements made using a miniature five-hole probe is provided here. A detailed description of the results can be found in references [2] and [3].

For the mean flow measurements presented here, a five-hole probe was used. A five-hole probe was chosen for its robust nature, reliable calibration, and for the pressure measurements that it provided in addition to velocity measurements. Caution must be used when utilizing a probe in a swirling flow because its introduction into the flow can create a local region of vortex breakdown if enough swirl is present. However, the flows investigated in this study did not contain enough swirl to induce vortex breakdown, so this type of probe interference was not expected here. As shown in Fig. 4(a), a 1.59mm (1/16th-inch) diameter five-hole probe with a hemispherical head was used to provide high-resolution flow-field measurements. The pressures from the five-hole probe were measured by a pressure transducer connected to the multiple pressure ports through a Scanivalve multiplexor. Voltages from the pressure transducer were digitized using a computer controlled A/D board, and the values were stored on a computer for later processing. Motion of the traverse system, monitoring of the conditions in the stilling chamber, and measurement of the five-hole probe pressures for both calibration and flow-field surveys were controlled using a LabView program.

The probe was fully calibrated in the swirling jet facility (in the absence of swirl) over a range of $\pm 35°$ in pitch and yaw in $5°$ increments. Zilliac's calibration method[4] was used to determine flow-field quantities from the measured pressures. In this approach, five pressures at the probe's tip are recorded at each calibration point.
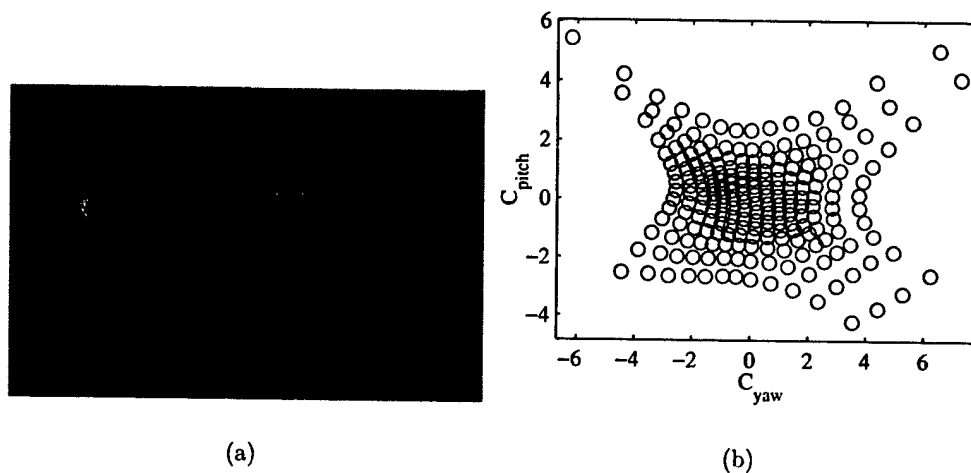
4

Figure 4: Five-hole probe: (a) Image of probe, and (b) example calibration.

Differences between these five pressures are then non-dimensionalized by the pressure difference between the central hole and the average of the four surrounding holes. These pressure differences yield local total pressure, static pressure, pitch, and yaw coefficients, two of which are shown in Fig. 4(b), that exhibit smooth behavior over the region calibrated. During a survey, the five probe pressures are measured and are used to calculate the non-dimensionalized coefficients. These coefficients are entered into a two-dimensional interpolation program that determines the flow-field quantities. Uncertainty in the measurements using the five-hole probe are discussed by Gilchrist and Naughton [2].

A primary need of this study was the creation of distinct tangential velocity profiles. Fig. 5 shows both axial and tangential velocity profiles for the five different swirling jets studied here. The swirling jet axial velocity profile exhibits a constant velocity across the jet exit, which is typical for well-conditioned jets. In contrast, the swirling jets show a "jet-like" profile at the exit, with the maximum velocity on the centerline. The q-vortex type swirling jets have a more pronounced peak in the center. Note that the conditions at the exit were set so that the average axial velocity at the exit was essentially the same. The tangential velocity profiles show that 2 distinct families of swirling flows have been generated. The solid-body type flows have a large region where the tangential velocity $\bar{w}$ is proportional to the radius. In contrast, the q-vortex type flows have a very small region with $\bar{w} \propto r$, reach their maximum tangential velocity at small r, and exhibit a slow tangential velocity decrease outside this region. Also evident from this figure is that different levels of swirl are present.

Although generating these profiles was a challenge, the intent of making mean flow-field surveys was to identify the effect of swirl on mixing, particularly the effect of swirl distribution. A detailed description of all the measurements made can be found in Gilchrist and Naughton [2], but the effect on growth enhancement is discussed briefly here.

5
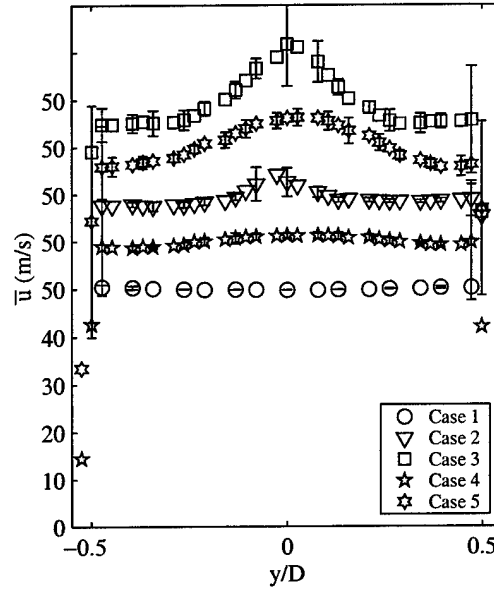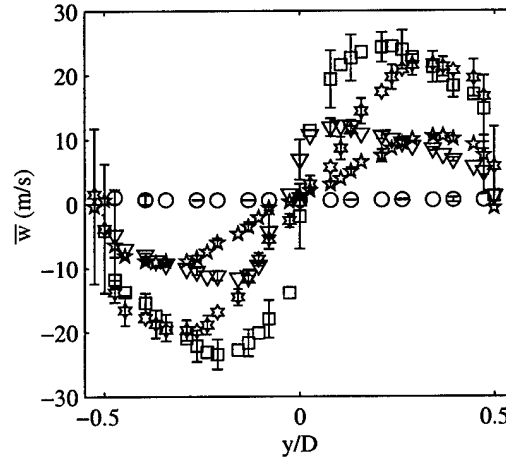
Figure 5: Mean velocity profiles at the jet exit: (a) axial velocity, and (b) tangential profile. Note that axial velocity profiles have been offset for clarity.

The centerline velocity decay is often used as a representation of how fast a jet is growing. Fig. 6 shows the results for the five cases studied here along with the results from some past studies. This figure indicates that the non-swirling and $S = 0.10$ swirling jets experience similar decay rates, whereas the $S = 0.22$ swirl cases exhibit a higher decay rate. The results in the present study agree well with those from the previous studies. One problem with using centerline decay rate is the non-uniform velocity at the jet exit for these swirling flows. The locally high centerline velocity at
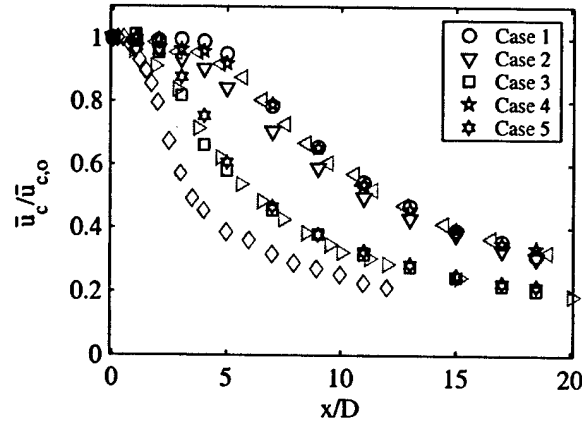
6

Figure 6: Centerline velocity normalized by the centerline velocity at the jet exit for the five different cases. The data shown in grey are from previous studies: ◁ - $S=0$, Rose [5]; ▷ $S=0.2$, Rose [5]; and ◇ - $S=0.48$, Farokhi et al. [6].

the exit may makes these results misleading. As a result, other measurements of jet growth were carried out.

As mentioned above, traditional methods of determining jet width often fail in swirling jet flows due to the complex axial velocity profiles associated with these flows. However, for axial locations with $x/D > 5$ (referred to as the developing region) where D is the jet diameter, the swirling jets relax toward axial profiles associated with a non-swirling jet. Fig. 7 shows the axial velocities non-dimensionalized by the jet half width b_{hw} (determined using a traditional sech^2 fit) and the centerline velocity. As is evident in the figure, the profiles collapse nicely at distances greater than four diameters downstream.

Since the jet profiles collapse when non-dimensionalized by b_{hw} for $x/D > 4$, b_{hw} is considered representative of the jet width in this region. Fig. 8 shows the variation of jet width with axial location for all five cases studied here. As is evident in this figure, all of the growth rates appear approximately linear in this region. The $S = 0.10$ swirling jets exhibit jet widths that are similar to those of a non-swirling jet. In contrast, the $S = 0.22$ swirling jets show a considerably larger jet width at each downstream location. In addition, the difference in the jet width for the $S = 0.22$ cases (cases 3 and 5) are virtually identical, regardless of the initial swirl distribution. These results enforce the view suggested by the centerline velocity decay that initial swirl distribution does not play a large role in determining the mixing enhancement observed in the developing region. This result is also supported by tangential velocity profiles (not shown here) that indicate that the velocity profiles begin to relax toward a similar distribution immediately downstream of the nozzle exit.

By fitting straight lines to the data in Fig. 8, growth rates can be determined. Fig. 9 shows the growth rates b'_{hw} non-dimensionalized by the growth rate of the non-swirling jet $b'_{hw,o}$ for the five cases studied here. In this figure, a value greater than one represents growth-rate enhancement. As expected, there is little enhancement
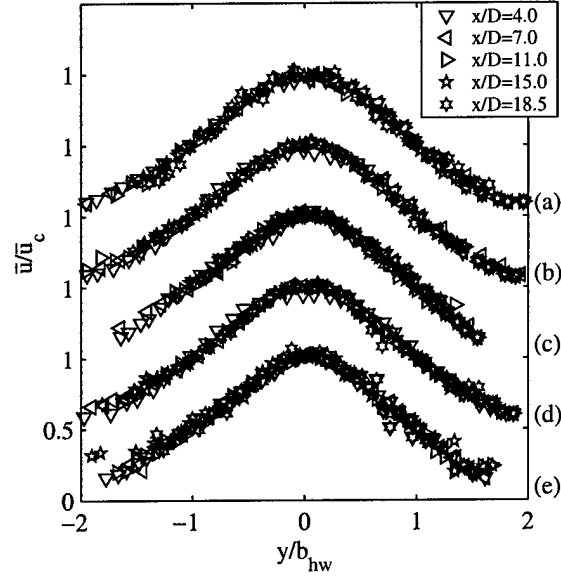
7

Figure 7: Normalized jet velocities using the half width (determined using sech^2 fit) to non-dimensionalize y. Note that each case is offset for clarity: (a) Case 1, (b) Case 2, (c) Case 3, (d) Case 4, and (e) Case 5.

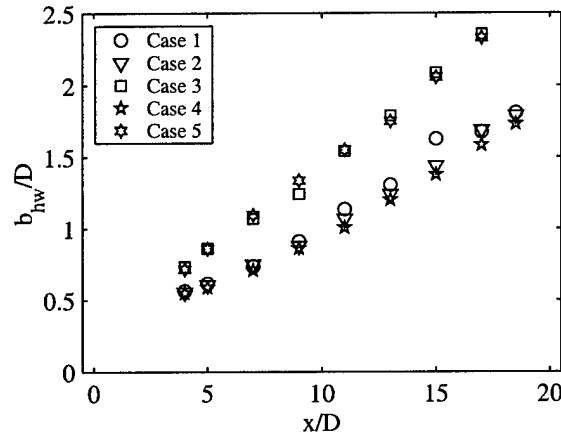Figure 8: Jet half width determined using sech^2 fit for the five different cases.

observed for the $S = 0.10$ swirling cases, and a significant amount of enhancement observed for the $S = 0.22$ swirling cases.

Fluctuating Flow-Field Measurements

The single-point fluctuating measurements are currently being analyzed, and a full description of the results will be provided in a later publication. However, a brief description of the fluctuating quantities at the jet exit is provided here to demonstrate the type of results that are expected. To further understand why swirling jets mix
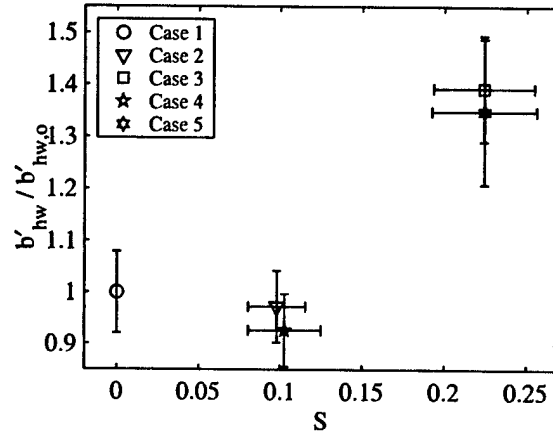
8

Figure 9: Normalized growth rate for the four swirling cases using the sech^2 method to define jet half widths.

faster than their non-swirling counterparts, the turbulence behavior of the different flows has to be considered. A first step in understanding the turbulence is to look at single-point statistical quantities: the normal and shear turbulence stresses and the auto- and cross-spectral density functions.

The calibration technique used for the cross wires is that suggested by Lueptow et al.[7]. This calibration process avoids some of the uncertainties that are inherent in a King's Law calibration process for cross wires. To calibrate the cross wire, it is inserted into the non-swirling jet flow, and voltages from the hot wires are obtained over a range of ±30° in pitch in 10° increments. This process is repeated at a number of velocities. Contour plots of u-velocity and w-velocity as a function of hot-wire voltages are shown in Fig. 10. By interpolating among the calibration points, the velocities corresponding to a particular voltage combination may be determined. The hot-wire voltages are temperature corrected to account for temperature variations during calibration and testing.

To determine the acquisition and filtering frequencies to use for sampling the cross wires in the swirling jet flow fields, two surveys were performed in the non-swirling jet: one survey used a sampling frequency of 50 kHz, a filtering frequency of 20 kHz, and a sampling period of 20 second, whereas the other used a sampling frequency of 5kHz, a filtering frequency of 2 kHz, and a sampling period of 50 seconds. Between these two surveys, fluctuations having low frequencies up to frequencies in the inertial range were acquired as evident in Fig. 11. These surveys indicated that there was little frequency content of interest below 50 Hz and that the inertial region of turbulence had been reached by 8 kHz as indicated by the 5/3 roll-off. Therefore, in the interest of time, a sampling frequency of 25 kHz, a sampling period of 5 seconds, and a filtering frequency of 10 kHz were chosen for the preliminary fluctuating measurements included here.

In order to ensure that the measurements using the five-hole probe and those made using the cross wires are performed in the same flow field, comparisons of the
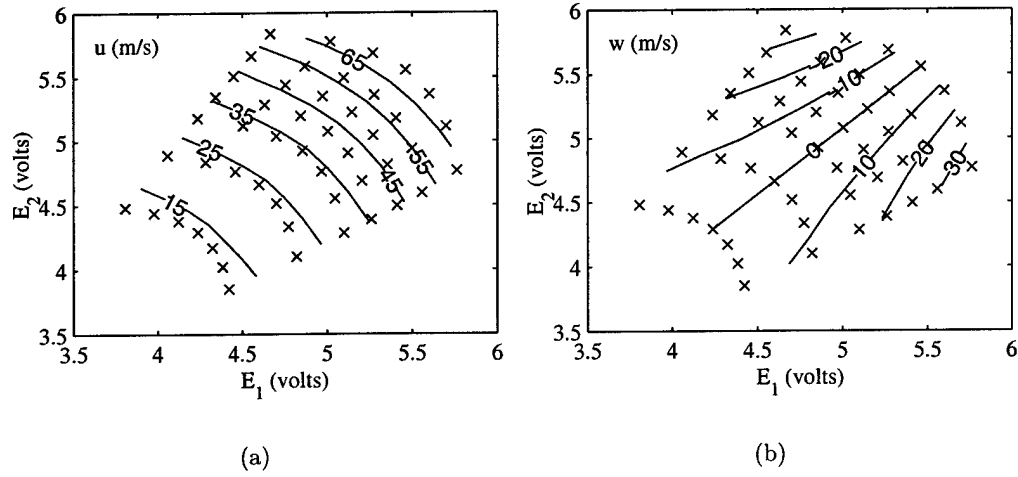
9

Figure 10: Cross-wire calibration: (a) u and (b) w.

mean velocities have been made at the nozzle exit. This comparison also serves to provide confidence in the measurements made using both instruments. The axial and tangential velocity profiles for the solid-body type swirl distributions with $S=0.23$ are shown in Fig. 12 in which it is evident that the agreement between the separate measurements is surprisingly good. All the other profiles show similar agreement.

Although the mean values determined from the cross-wire measurements are encouraging, these measurements are primarily used to investigate turbulence statistics. In Fig. 13, the turbulent normal and shear stresses are shown for all five cases at the nozzle exit. Note that the turbulent normal stresses have been non-dimensionalized by the centerline axial velocity $\bar{u}_c$, but the turbulence shear stress is normalized by $\bar{u}_c^2$ due to the sign change in the data. It is obvious from this figure that the addition of swirl significantly increases both turbulent normal stresses and the turbulent shear stress. For a given value of S, the axial shear stresses are highest in the core (near $y/D = 0$) for the q-vortex type distribution, whereas the solid-body type distribution has the highest $\sqrt{\overline{u'^2}}/\bar{u}_c$ values away from the core. Recall that, near $y/D = 0$, the q-vortex type distribution has high gradients in both tangential and axial velocities thus explaining the high turbulence intensities found there. However, the axial velocity gradients $(\partial\bar{u}/\partial r)$ across the solid-body type swirling jet are not high thus suggesting that the energy found in $\sqrt{\overline{u'^2}}/\bar{u}_c$ is gained by redistribution from the other normal and shear turbulent stresses. The behavior of the tangential turbulent normal stress is similar, but the levels are consistently higher than the axial component. In particular, the $\sqrt{\overline{w'^2}}/\bar{u}_c$ values for the q-vortex type swirl distribution have a very high peak in the core. The $\sqrt{\overline{w'^2}}/\bar{u}_c$ values for the solid-body cases are approximately double the axial values for the $S = 0.23$ case and show an even greater increase for the $S = 0.10$ case. The turbulent shear stress $\sqrt{\overline{u'w'}}/\bar{u}_c^2$ again shows a similar behavior to the solid-body type swirl exhibiting higher values in the outer region and the

10
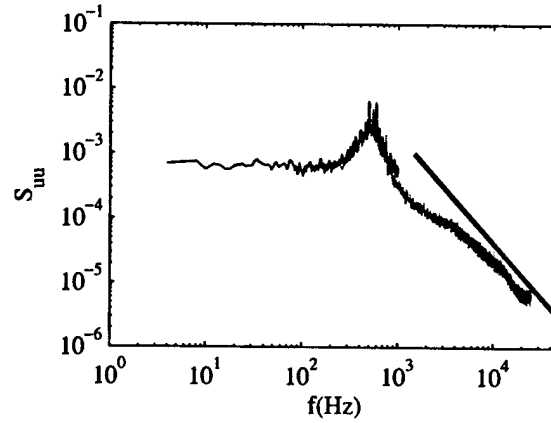
(a)
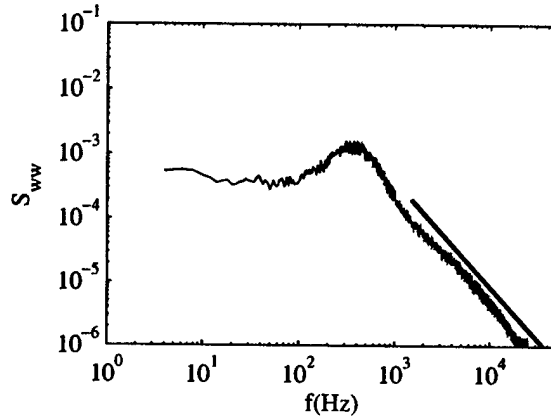
(b)

Figure 11: Comparison of auto-spectral density function calculated using different data sets with different sampling rates taken in a non-swirling jet on the centerline: (a) auto-spectral density function of streamwise fluctuations and (b) auto-spectral density function of tangential fluctuations. The data set taken at a lower sampling rate is shown in black, and the data set taken at the higher sampling rate is shown in gray. A line with a slope of -5/3 is shown for reference.

q-vortex type distribution showing the highest values in the core. The sign change across the core is expected since the mean axial velocity is in the same directions on both sides of the core, whereas $\bar{w}$ switches sign (Note that $\overline{u'v'_\theta} = |\overline{u'w'}|$). It should be noted that, for all turbulence normal and shear stresses shown, the values for the non-swirling jet are very low. This is expected since the swirling jet facility has been designed to produce a low turbulence jet at the exit.

The results presented in Fig. 13 reveal some phenomena related to swirling jets that may be responsible for the mixing enhancement observed in these flows. First, the swirling jets have a built-in turbulence production mechanism - the mean shear provided by the mean tangential velocity distribution. The swirling jets already have

11
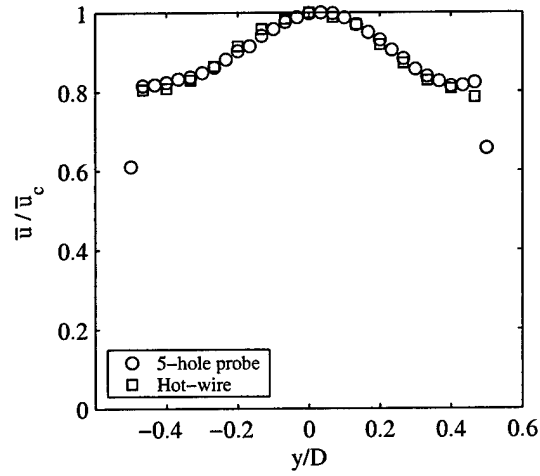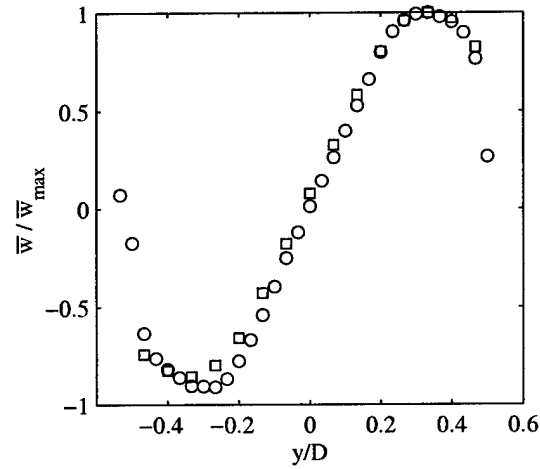
Figure 12: Comparison of solid-body S=0.23 swirling jet profiles determined using five-hole probe and cross-wire anemometry: (a) axial velocity profile and (b) tangential velocity profile.

significant turbulence levels at the jet exit and are not relying on an interaction with the surrounding air to produce turbulence. It should be emphasized here that the present study has clearly shown that the enhanced turbulence levels at the exit are not a by-product of the swirl production method as has been suspected in previous studies. The results here provide initial evidence for the increased mixing observed, but an understanding of the rapid increase in mixing at $x/D \sim 5$ must await analysis of measurements made in that region.

Further insight into the reasons for mixing enhancement observed in swirling jets can be obtained by looking at turbulent spectra. At the nozzle exit, non-swirling
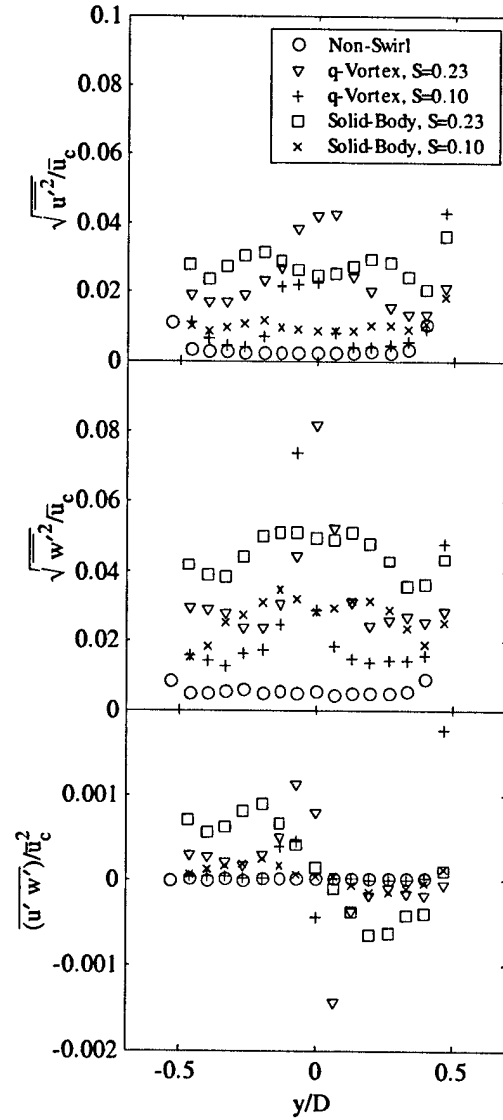
Figure 13: Profiles of fluctuating velocities at the nozzle exit: (a) axial turbulence intensity (b) tangential turbulence intensity, and (c) non-dimensional Reynolds stress.

jets exhibit spectra with few extraordinary features. How are the spectra changed by the addition of swirl? Fig. 14 shows the auto-spectral (S_{uu} and S_{ww}) and cross-spectral (S_{uw}) density functions for all five cases studied at the nozzle exit at radial locations y/D=0.27. The spectra shown have been averaged from 100 individual spectra and have a frequency resolution of 20 Hz. Note that a wider range of frequency capturing the behavior at lower and higher frequencies would have been preferred, but the present results serve for an initial comparison. As suggested by the turbulent
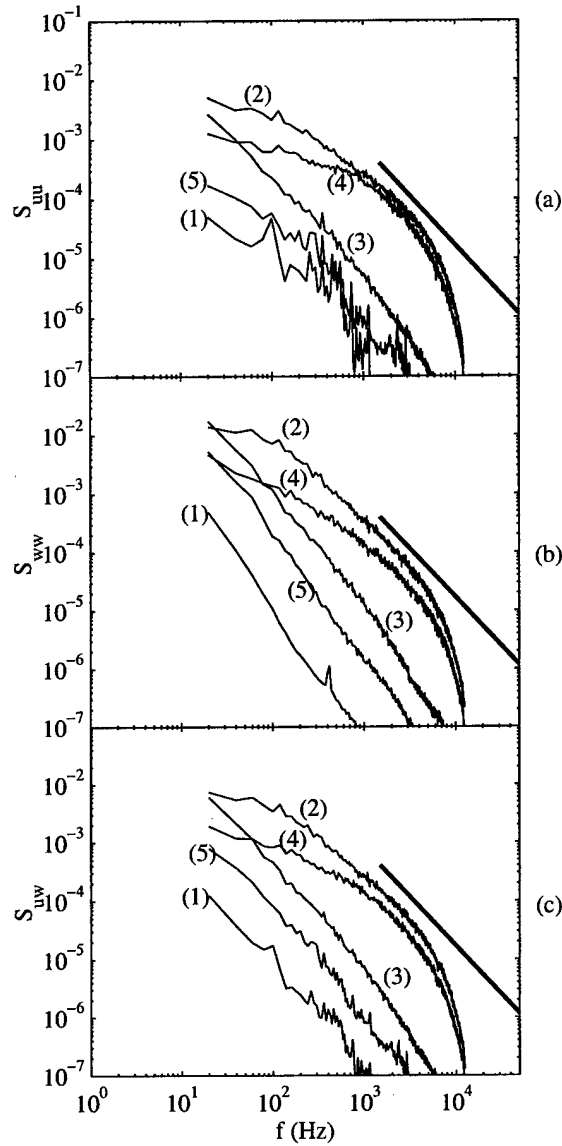
13

Figure 14: Auto- and cross-spectral density functions of fluctuations at $x/D = 0.54$ for different types of swirl: (1) no swirl, (2) solid body, S=0.23, (3) solid body, S=0.10, (4) q-vortex, S=0.23, and (5) q-vortex, S=0.10. Three spectra are shown: (a) auto-spectral density function of axial fluctuations S_{uu}, (b) auto-spectral density function of tangential fluctuations S_{ww}, and (c) axial-tangential cross-spectral density function S_{uw}.

stresses, the magnitudes of the spectral density functions for the swirling jets are orders of magnitude higher than those of the non-swirling jet. In addition, all three spectra for each of the five cases behave similarly at a given location.

14

At different radial locations, the behavior of the spectra changes for the different swirl profiles and strengths. Here, the spectra at y/D=0.27 are discussed. The solid-body type distribution has the greater magnitudes for both the higher and lower swirl cases. In this region, the tangential velocity for the q-vortex type profile is at or just past its maximum value, and the gradients are low. In contrast, the velocity for the solid-body profile case continues to increase in this region, and the gradient is unchanged from the value in the core. However, since the swirl profile is solid body, no mean tangential shear is present at this point. One notable feature of the $S = 0.23$ cases is that there is a rapid roll-off in the magnitude of the spectra at higher frequencies. The cause for this roll-off is not known at this time.

There are several observations that can be made from spectra such as that shown in Fig. 14. In the non-swirling jet, the spectra magnitudes are very low, and there are no spectral features evident. Although the spectra magnitude appear to increase with swirl exponentially, no dominant peak is obvious for these cases over the frequency range measured. As would be expected, the magnitudes across the entire spectrum are elevated in magnitude in the regions of highest shear (e.g. the core for the q-vortex type swirl distribution). However, the magnitude of the spectra are still elevated across the entire jet width for the solid-body type distribution where mean shear is absent. Finally, for several of the profiles, a very high roll-off in the spectra magnitude is evident, and higher frequency measurements are needed to resolve this issue.

Swirling Jet Measurements Summary

The primary finding in this portion of the study is that the addition of swirl increases jet growth rate regardless of initial swirl profile if the swirl is sufficiently large. The enhanced growth rates appear to be largely independent of the initial swirl profile, although the effect of the distribution on the near field growth was not studied in detail here. Growth rate enhancements up to 40 % were observed for the cases studied here. Centerline velocity decay rates also agree with past studies. Measurements at the nozzle exit indicate the highest swirl cases have elevated turbulence levels, and analysis of turbulence measurements at locations further downstream are currently underway.

Synthetic Jet Control of a Turbulent Mixing Layer

The active control portion of this project explored the interaction of a synthetic jet actuator with a developing free shear layer. The turbulent structure in a shear layer consists primarily of spanwise vortices, but this structure is augmented by a secondary structure of streamwise-aligned vortices. The origin of the spanwise structure is well known to be a consequence of the Kelvin-Helmholtz instability. The secondary structure, on the other hand, does not arise from an instability, but rather from three-dimensional disturbances present in the upstream flow. Previous work has revealed that the introduction of streamwise vorticity to the upstream boundary layer, through passive means say, can enhance the mixing in a shear layer in the early stages of its development[8]. A synthetic jet issuing normally into a cross-flow boundary layer has been shown to create streamwise-aligned vortices in the boundary layer[9, 10]. In this study, we placed a synthetic jet actuator near the trailing edge of a splitter
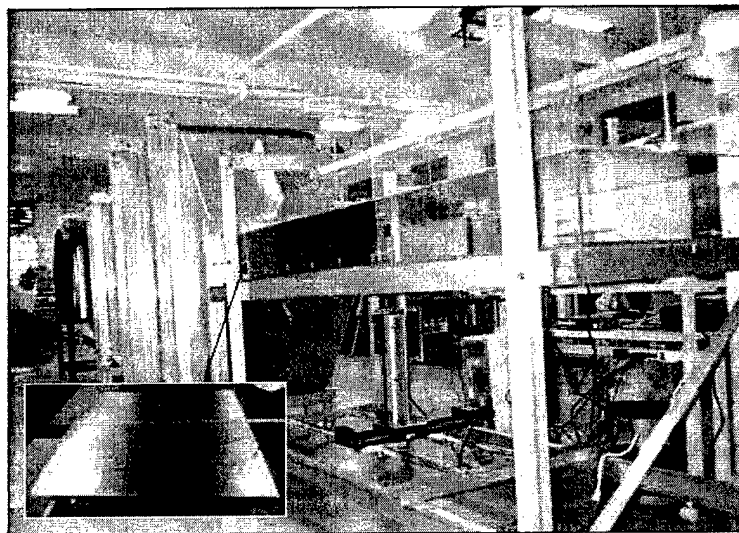
15

Figure 15: A view of the wind tunnel test section (looking upstream). Inset shows the splitter plate that is mounted in the contraction section of the wind tunnel.

plate that was used to form a shear layer. The objective of this work was to study how the interaction of the synthetic jet with the cross-flow on the high-speed side of the splitter plate impacted the subsequent development of the mixing layer and the turbulent structure therein. Of particular interest was how the vortices from the synthetic jet interact with the streamwise vortices that naturally occur in the mixing layer and to what extent the mixing layer growth was altered by this interaction.

Experimental Setup

The experiments were performed in a low-speed, blower wind tunnel at the University of Wyoming (figure 15). A splitter plate (figure 15) was mounted in the contraction section of the wind tunnel and divided the section into equal sections upper and lower. The splitter plate ended at the entrance to the test section. A head loss device was mounted in the lower section of the contraction, near the leading edge of the splitter plate and upstream of the beginning of the contraction. It consisted of six layers of furnace filter material. The velocities of the high- and low-speed streams were measured at 38 m/s (U_h) and 27 m/s (U_l), respectively. These velocities give a velocity ratio of 0.71, a convection velocity of $U_c = 32$ m/s and a characteristic velocity difference of $U_s = \Delta U = 11$ m/s.

The synthetic jet actuator used in the study was a resonating cavity device driven with a single piezoelectric disk mounted opposite the orifice. The actuator orifice was rectangular and measured 25.4 mm by 0.50 mm. Two orientations of the actuator orifice were used. One orientation was with the major axis of the orifice aligned in the spanwise direction (actuator 1) and the other orientation was with the axis oriented in the streamwise direction (actuator 2). The maximum jet velocity was found experimentally to occur an actuator driving frequency of 1.1 kHz. This actuator frequency was higher than the unstable frequency of the mixing layer, and consequently, the

input to the flow appeared steady. The actuator was placed near the trailing edge of the splitter plate just upstream of where the plate begins to taper to the sharp trailing edge. To position the synthetic jet actuator close to the splitter plate trailing edge, it was necessary to maintain the plate thickness as far aft on the plate as possible. Consequently, the plate tapered to the sharp trailing edge with a relatively steep (7°) angle.

Mean and fluctuating velocity measurements were obtained using both a pitot tube and a cross-wire probe. The cross-wire probe was calibrated using the routines of Lueptow et al.[7] and Bell and Mehta[11]. The cross-wire measurements were made with the probe in two orientations, one for U and V velocities and one for U and W velocities. At each survey point, we also obtained the Reynolds normal stresses and two components of the Reynolds shear stress. In all surveys, the dynamic pressure in the high-speed stream and the mean flow temperature were measured. The latter measurement was used to correct the hotwire voltages for temperature drift. An automated, 2-D traverse was used to obtain measurements in Y-Z planes at fixed streamwise locations. The data was taken at five different streamwise locations in the mixing layer. A sixth set of surveys was taken on the splitter plate, downstream of the actuator, to study the effect of actuator on the boundary layer.

In the experiments, the origin of the reference coordinate system was located at the trailing edge of the splitter plate with X measured in the streamwise direction, Y measured in the cross-stream direction and Z measured in the cross-span direction. All cross-wire measurements were obtained on a rectangular grid that spanned between ±22.5 mm in Z. In the Y direction, the grid points were equally spaced at intervals of 1 mm, and in the Z direction points were spaced at 1.5 mm.

Experimental Results

We have examined the Reynolds stress distributions obtained from the cross-wire measurements at six streamwise locations with and without control. The focus of the measurements was on identifying streamwise vortices in the mixing layer and evaluating how the control changes the distribution of these vortices. Bell and Mehta[12] have shown that the secondary Reynolds shear stress, $\overline{u'w'}$, is an effective indicator of both the strength and position of streamwise vortices in turbulent mixing layers. Consequently, in the following discussion, we use contours of this stress to evaluate the effect of control on the streamwise vortices. We will also show contours of the streamwise normal stress distributions, $\overline{u'^2}$, to reveal how the control modified the cross-span profile of the mixing layer.

Secondary Shear Stress Measurements To characterize the actuator input to the splitter plate boundary layer, one set of data was obtained at X = -5 cm on the splitter plate and just downstream of the actuator. The secondary Reynolds shear stresses for this location are shown in figures 16(a), 17(a) and 18(a). For the unforced case (figure 16a), the contours are uniform across the span indicating that the plate boundary layer is two-dimensional. Figure 17(a) shows a region of reduced stress immediately aft of actuator 1. For actuator 2 (figure 18a), the jet rapidly penetrates deep into the cross-flow and is distorted to become quite larger in the cross-span

17

(a) X=-5cm

(b) X=7.5cm
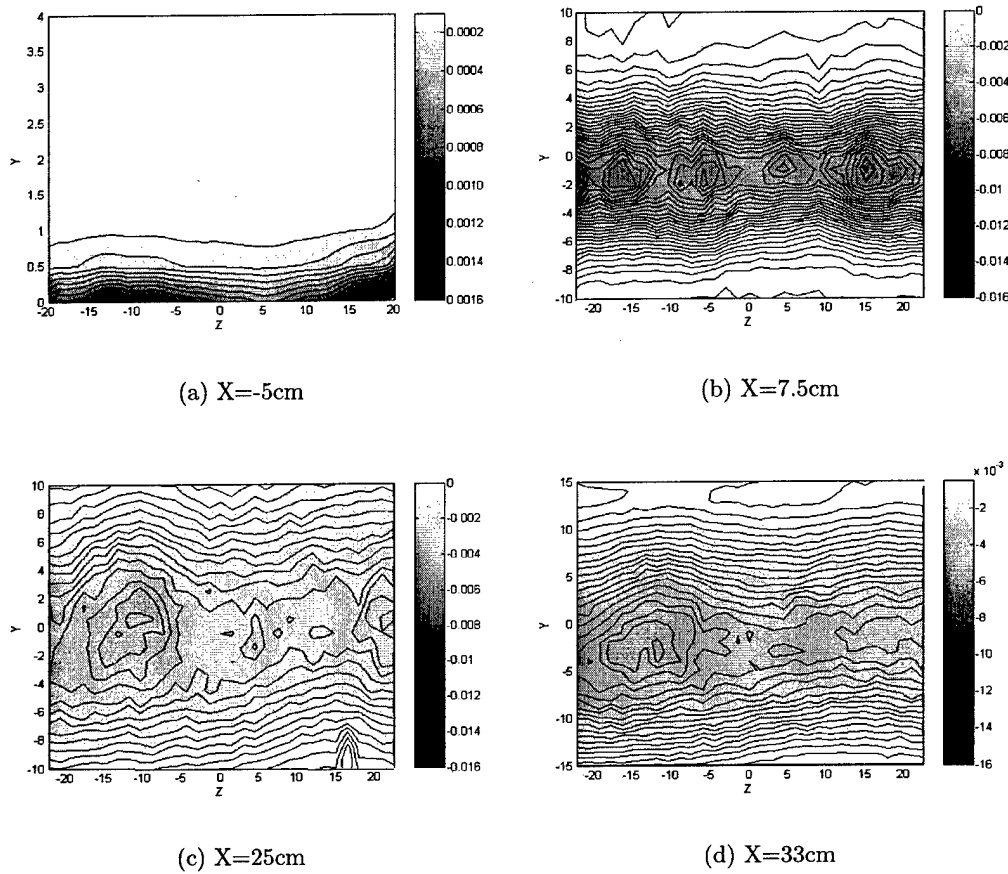
(c) X=25cm

(d) X=33cm

Figure 16: Contours of the secondary Reynolds stress, $\overline{u'w'}$ for the mixing layer without forcing.

direction that the actuator orifice width would suggest. Although we cannot infer a distinct structure in the boundary layer from these measurements, it is clear that, in both cases, the synthetic jet has significantly modified the boundary layer turbulence in its wake.

Contours of the secondary shear stress for all three cases and for three of the six streamwise measurement locations are shown in figures 16-18. For the unforced case at X=7.5 cm (figure 16b), we can see small concentrations of $\overline{u'w'}$, and from these concentrations, we can infer the existence of four streamwise vortices centered around Z=0. The sizes of the vortices are comparable and approximately 2 mm in diameter. Moving downstream, these vortices grow and merge.

Contours of the secondary shear stress with actuator 1 (cross-span orientation) are shown in figure 17. At X=7.5 cm (figure 17b), we observe a more clearly defined structure than in the unforced case with higher levels of the secondary shear stress. The contours suggest the presence of three well-defined vortices that are larger in

18
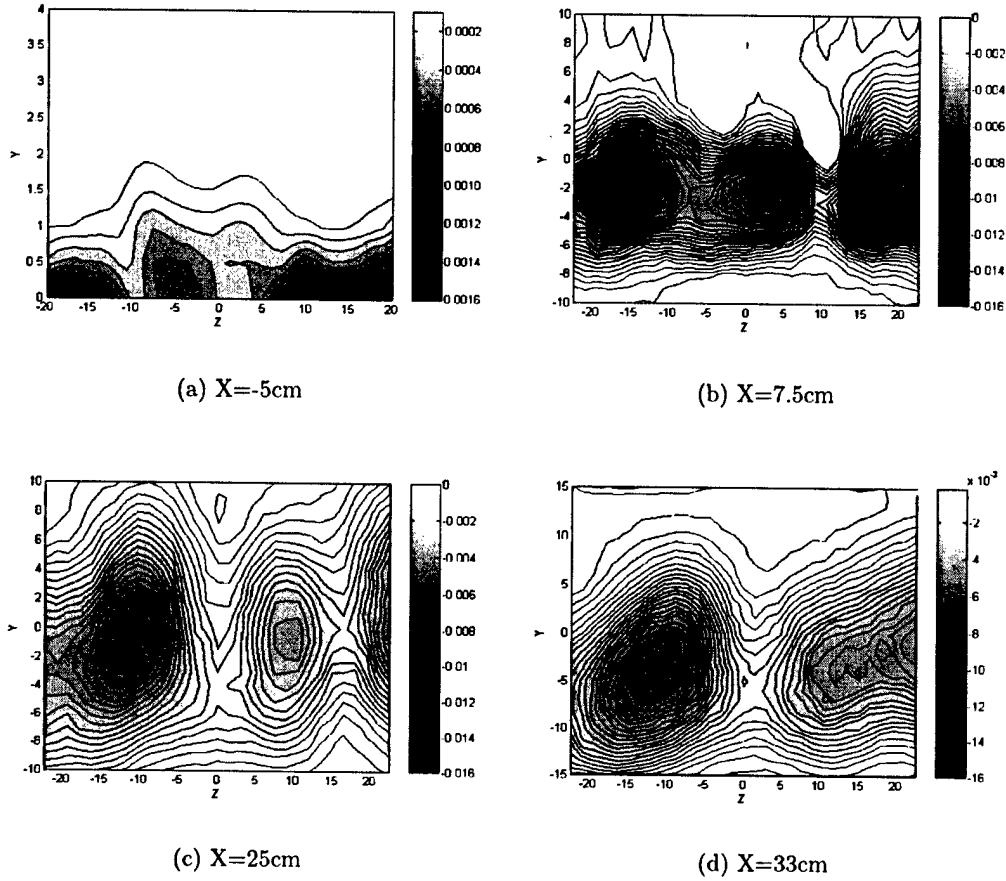
(a) X=-5cm

(b) X=7.5cm

(c) X=25cm

(d) X=33cm

Figure 17: Contours of the secondary Reynolds stress, $\overline{u'w'}$ for the mixing layer with actuator 1.

scale than in the unforced mixing layer. The vortex at $Z = 17$ mm appears to be interacting with a neighbor just outside the measurement domain and at subsequent downstream locations, the vortex appears larger in scale suggesting that merging has taken place. In figures 17(c)-(d), we observe the merging of two vortices for $Z > 0$ and a slight drift of the vortices to increasing values of Z.

Figures 18 show the secondary shear stress contours for actuator 2. Comparing this forced case to the unforced mixing layer, the $\overline{u'w'}$ contours at X = 7.5 cm appear similar although with higher peak values. We can identify three, possibly four, streamwise vortices. There is a slight distortion apparent on the low-speed side of the mixing layer. This concave distortion becomes increasingly apparent farther downstream. Between X=25 cm and X=33 cm, we see two of the vortices in the mixing layer begin to merge, and at X = 33 cm, a third vortex appears to have wrapped into the merging and the overall shape of the $\overline{u'w'}$ contours becomes elliptical. The peak shear stress levels are higher in this forcing case than in the unforced case, and it ap-

19

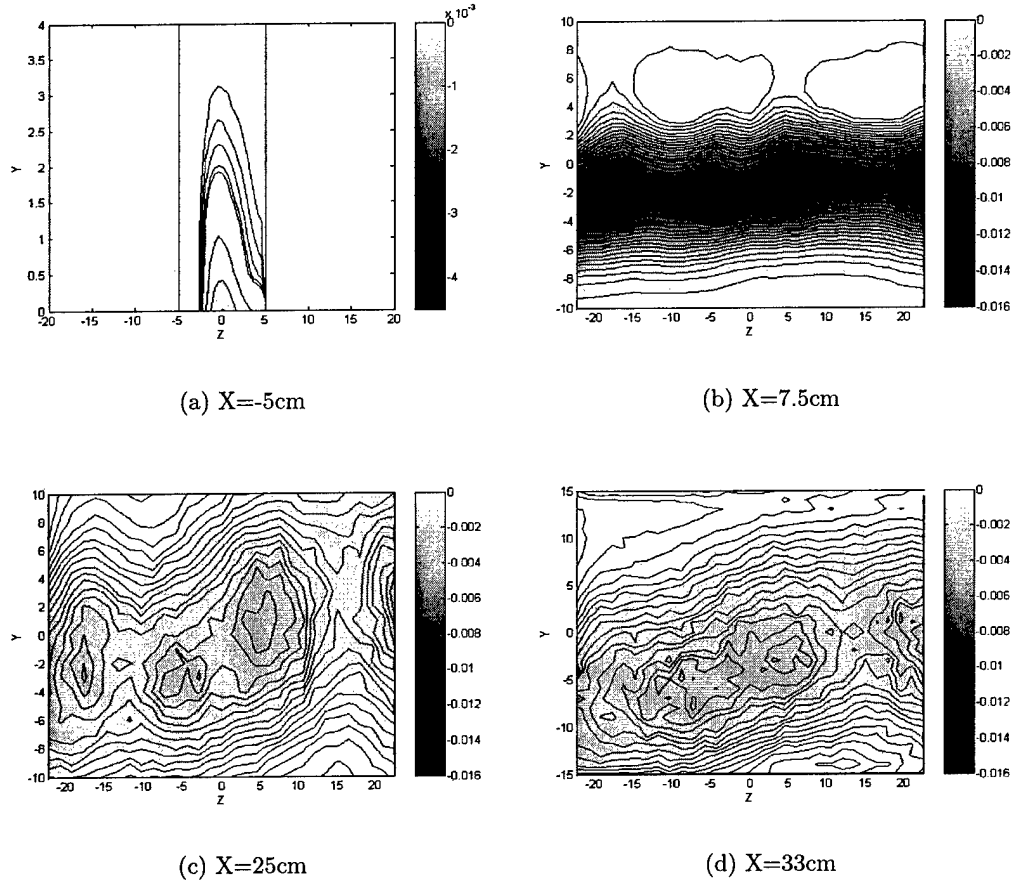(a) X=-5cm

(b) X=7.5cm

(c) X=25cm

(d) X=33cm

Figure 18: Contours of the secondary Reynolds stress, $\overline{u'w'}$ for the mixing layer with actuator 2.

pears that these higher stress levels are associated with stronger streamwise vortical motions.

From the measurements, we can conclude that streamwise vortices are present in the unforced mixing layer in small sizes and irregular arrays initially, and with increasing downstream distance, they grow in size, perhaps through merging, and retain their coherence. Comparing the stress contours for the three cases, it is clear that the introduction of control with actuator 1 increases the size and enhances the coherence of streamwise vortices in the mixing layer. At X=7.5 cm, the average diameter of the streamwise vortices without control was approximately 2 mm. With control from actuator 1, this diameter appeared to increase by almost a factor of two. In contrast, the input from actuator 2 appears to have a smaller effect on the size of the vortices in mixing layer. At X = 7.5 cm, the streamwise vortices for the actuator 2 case are approximately the same size as for the unforced case although in the forced case the vortices appear elongated in the cross-span direction. Farther downstream,

20

however, the distortion of the mixing layer by actuator 2 becomes apparent, and this distortion was not observed in the unforced case. Finally, in both forcing cases, the peak shear stress levels are higher than in the unforced case. This observation suggests that not only may the vortices be larger and more coherent but also stronger. In the case of actuator 2, we observed at distortion of the mixing layer across the span, and the shapes of the shear stress contours for actuator 1 also suggest a severe distortion of the layer.

Streamwise Normal Stress Measurements To illustrate the distortion of the mixing layer as a result of the stronger and more coherent streamwise vortices, we consider contours of the streamwise Reynolds normal stress, $\overline{u'^2}$. Figure 19(a)-(b) shows the streamwise normal stress contours for the unforced case at X = 7.5 cm and X = 33cm. In this case, the relatively weak streamwise vortices do not distort the cross-span profile of the mixing layer, and the layer is nominally two-dimensional.

The streamwise normal stress for the two forced cases are shown in figures 19(c)-(d) and 19(e)-(f). In a comparison of the $\overline{u'^2}$ contours for the three cases at X = 7.5 cm (figures 19a,c,e), there is little apparent change in the contour values with the introduction of the actuator input. The maximum normalized $\overline{u'^2}$ values in all the three cases are approximately 0.064. Moving downstream, however, for actuator 1 a distortion of the mixing layer becomes apparent. Comparing the secondary shear stress contours at X = 33 cm (figure 17d) with the distortion in the Reynolds normal stress contours at the same location, we can infer that the structure associated with the shear stress contours for Z < 0 is a counter-clockwise rotating streamwise vortex. For actuator 2, the normal stress contours also reveal a cross-span distortion of the mixing layer although of apparently much larger span and not as pronounced as the effect from actuator 1.

Mixing Layer Thickness and Growth To further illustrate how the actuator affects the mixing layer shape in the cross-span direction, we consider the variation in the mixing layer thickness, δ, across the span. The values of δ, for the three cases, were obtained from the $\overline{u'^2}/U_s^2$ measurements. Using $\overline{u'^2}/U_s^2 = 0.02$ to denote the mixing layer edges, the thickness of the layer was estimated at each spanwise measurement location. Figure 20 shows the variation in the mixing layer edges across the span for all three cases and at X = 7.5 cm and 33 cm. Without the actuator input, the mixing layer thickness is relatively constant across the span. The introduction of control gives a noticeable distortion to the mixing layer across the span beyond X = 7.5 cm, but initially there is no apparent effect. Apparent in the figure 20(b) is the distortion of the mixing layer by the strong vortices produced by actuator 1. This distortion does not appear to change the local mixing layer thickness across the span, since the crests on the high-speed side match with the troughs on the low-speed side, thus keeping the mixing layer thickness almost the constant. The distortion is otherwise consistent spatially and appears to be amplified with streamwise distance as a result of the increase in the size of the streamwise oriented vortices. At X = 33 cm with forcing from actuator 2, the mixing layer increases in thickness with
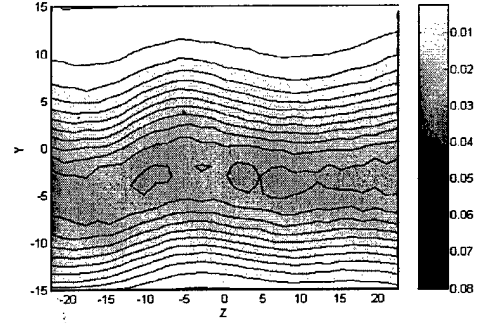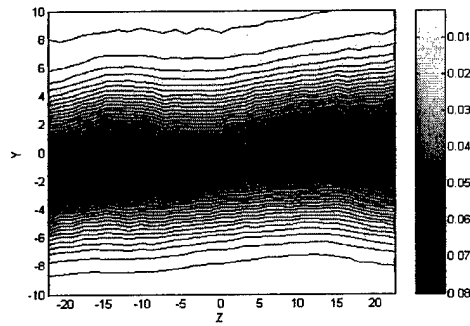
21
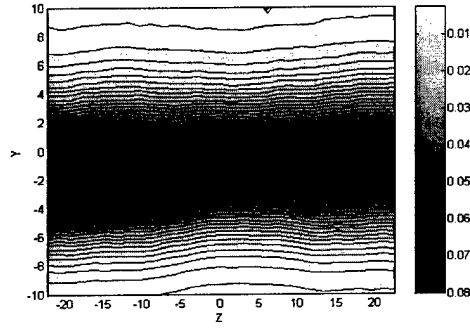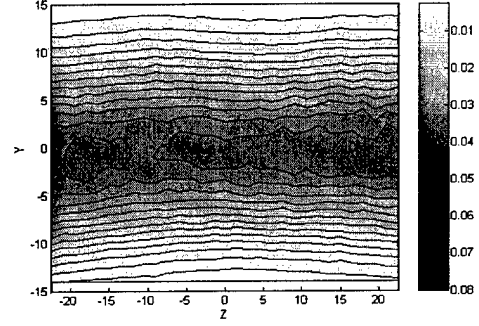
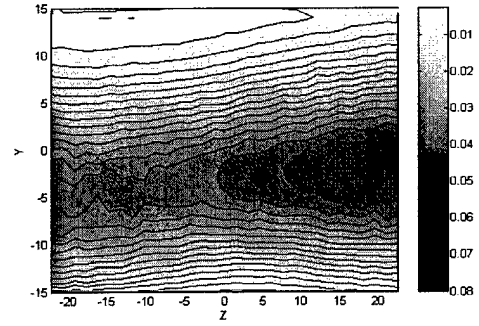(a) unforced, X=7.5cm

(b) Unforced, X=33cm
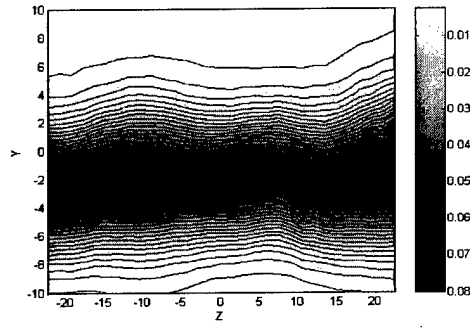
(c) Actuator 1, X=7.5cm

(d) Actuator 1, X=33cm

(e) Actuator 2, X=7.5cm

(f) Actuator 2, X=33cm

Figure 19: Contours of the streamwise normal Reynolds stress, $\overline{u'^2}$ for the mixing layer.
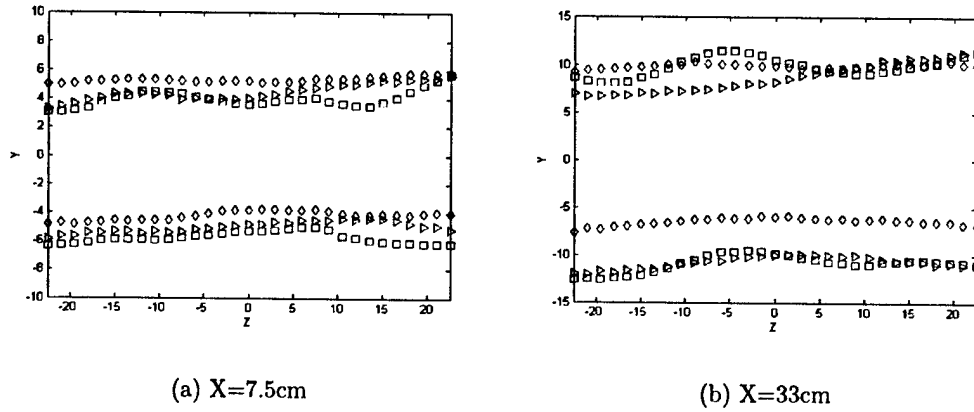
(a) X=7.5cm

(b) X=33cm

Figure 20: The spanwise variation in the mixing layer thickness, δ, at different streamwise locations: $\Diamond$, unforced; $\Box$, actuator 1; $\triangleright$, actuator 2.
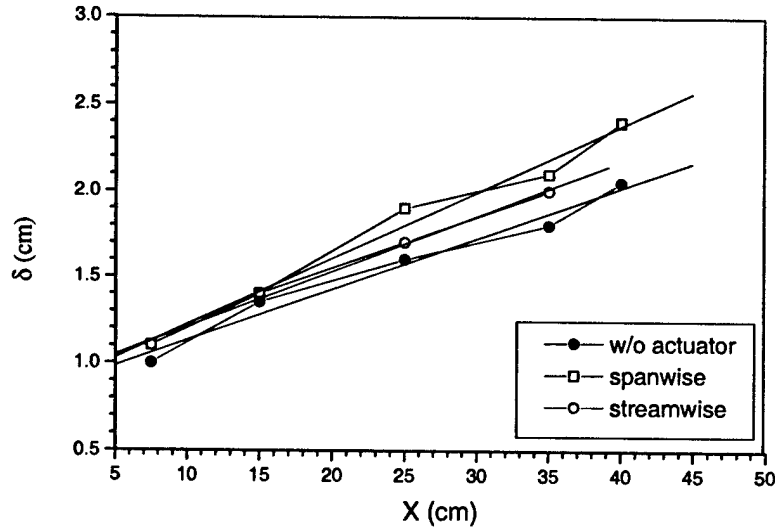

Figure 21: Streamwise variation in the mixing layer thickness: $\bullet$, unforced; $\Box$, actuator 1; o, actuator 2. The lines are linear fits to the data.

increasing Z. Coupling this observation with the shapes of the shear stress contours (figure 18) suggests that the effect of actuator 2 is a distortion to the mixing layer with a larger spanwise dimension than with control from actuator 1. Moreover, the distortion appears to be centered near Z = 25 cm with half of the distorted mixing layer lying outside of the measurement domain.

The growth of the mixing layer for all three cases is illustrated in figure 21. In these cases, the mixing layer thickness was obtained from a cross-span spatial mean. For the unforced case, despite some scatter in the data, the mixing layer thickness, δ, increases linearly with streamwise distance, and the non-dimensional growth rate,

$\left(\frac{U_c}{U_s}\frac{d\delta}{dx}\right)$, is 0.077, which agrees well with established growth rates for self-similar mixing layers. The non-dimensional growth rate increases to 0.118 for actuator 1 and 0.092 for actuator 2 and appears to retain the linear growth behavior, which is consistent with the nominally self-similar velocity profiles (not shown). This mean behavior reveals that with forcing from actuator 1 the local growth rate of the mixing layer increased by 53%, but only increased by 19% with forcing from actuator 2.

Ongoing Work

Two-point turbulence measurements in the swirling jets are currently underway and should yield data necessary to identify changes in turbulence structure. The POD (Proper Orthogonal Decomposition) modes will be determined using these data and will be used to identify large changes in the turbulent structure.

To investigate the hybrid control of jet flows, an assembly has been constructed that integrates four synthetic jet actuators around the periphery of the swirling flow. The assembly is shown schematically in Fig. 22(a), and an image of the hardware is shown in Fig. 22(b). The assembly holding the synthetic jets slides over the nozzle mounted to the swirling jet facility. The end of the existing nozzle mates smoothly with the collar holding the four synthetic jets that are oriented every 90°. One of the synthetic jet orifices (oriented in the stream wise direction) is evident in the figure. Testing of hybrid flow control using this hardware has been delayed awaiting completion of the swirling jet characterization. Without characterizing the swirling jet completely, successful hybrid control would be fortuitous.

Personnel

- The Principal Investigators for this study are **Jonathan W. Naughton** (Ph.D., Pennsylvania State University) and **Douglas R. Smith** (Ph.D., Princeton University). They are both faculty members at the University of Wyoming.

- **Surajeet Ghosh** (UW Graduate Student) worked on the active control effort. He designed and led the construction of the shear layer wind tunnel described above.

- **Robert Gilchrist** (UW Graduate Student) has been involved in the design of both the swirling jet and the traverse system. Robert also fabricated and calibrated a five-hole probe for mean flow-field surveys in the jet. In addition, Robert obtained single-point cross-wire surveys of the jet, which were completed this spring and are currently being analyzed. Robert has finished his research work and is currently writing his thesis.

- **Shane Buller** (UW undergraduate) and **Adam Martens** (UW undergraduate) were involved in the design and construction of the swirl injector and traverse system.

- **Torben Grumstrup** (UW undergraduate) designed and oversaw the fabrication of the synthetic jet collar for the jet facility.
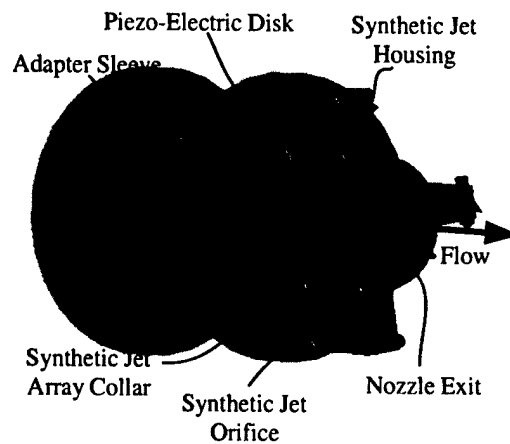
(a)

(b)

Figure 22: Integration of an array of synthetic jets with the swirling jet: (a) schematic and (b) image of the hardware.

- **James Robinson** (UW undergraduate) is currently making two-point cross-wire measurements in the swirling jet facility.

Degrees Obtained

Surajeet Ghosh, M.S. 2002, Thesis title: *A study of the effect of a synthetic jet on the near-field development of a turbulent mixing layer*

Publications Resulting from this Work

Journal Articles

1. R. T. Gilchrist and J. W. Naughton, "An experimental study of incompressible swirling jets with different initial swirl profiles: Mean results," submitted to *AIAA Journal* for publication.

Conference Papers

1. R. T. Gilchrist and J. W. Naughton, "An experimental study of swirling jets with different initial swirl profiles," AIAA Paper 2003-0639, 41st Aerospace Sciences Meeting and Exhibit, Reno, NV, January 2003.

2. R. T. Gilchrist and J. W. Naughton. " The design of a swirling jet facility," AIAA Paper 2002-0442, 40th AIAA Aerospace Sciences Meeting and Exhibit, Reno, NV, January 2002.

3. S. Ghosh and D. Smith, "The Effect of a Synthetic Jet on the Near-Field Development of a Turbulent Mixing Layer," AIAA Paper 2002-2824, 1st AIAA Flow Control Conference, June 2002.

Abstracts

1. R. Gilchrist and J. W. Naughton. "Generation of jet flows with arbitrary swirl profiles," *Bulletin of the American Physical Society*, (10), 157, November 2001.

Acknowledgement/Disclaimer

References

[1] R. T. Gilchrist and J. W. Naughton. The design of a swirling jet facility. AIAA Paper 2002-0442, January 2002.

[2] R. T. Gilchrist and J. W. Naughton. An experimental study of swirling jets with different initial swirl profiles. AIAA Paper 2003-0639, January 2003. 41st Aerospace Sciences Meeting and Exhibit, Reno, NV.

[3] R. T. Gilchrist and J. W. Naughton. An experimental study of incompressible swirling jets with different initial swirl profiles: Mean results. 2003. submitted for publication.

[4] G .G. Zilliac. Modelling, calibration, and error analysis of seven-hole pressure probes. *Experiments in Fluids*, 14:104–120, 1993.

[5] W. G. Rose. A swirling round turbulent jet. *Journal of Applied Mechanics, ASME Transactions, Series E*, 84:615–625, December 1962.

[6] S. Farokhi, R. Taghavi, and E. J. Rice. Effect of initial swirl distribution on the evolution of a turbulent jet. *AIAA Journal*, 27:700–706, June 1989.

[7] R. M. Lueptow, K. S. Breuer, and J. H. Haritonidis. Computer-aided calibration of x-probes using a look-up table. *Experiments in Fluids*, 6:115–118, 1988.

[8] J.H. Bell and R.D. Mehta. Interaction of a streamwise vortex with a turbulent mixing layer. *Physics of Fluids A*, 2:2011–2023, 1990.

[9] D. R. Smith. The interaction of a synthetic jet with a cross-flow boundary layer. *AIAA Journal*, 40(11):2277–2288, 2002.

[10] A. B. Bridges and D. R. Smith. Influence of orifice orientation on a synthetic jet - boundary layer interaction. *AIAA Journal*, 2003. To appear.

[11] J.H. Bell and R.D. Mehta. Three-dimensional structure of plane mixing layers. Technical Report JIAA TR-90, Joint Institute of Aeronautics and Acoutics, Stanford University, March 1989.

[12] J.H. Bell and R.D. Mehta. Measurements of streamwise vortical structures in a plane mixing layer. *Journal of Fluid Mechanics*, 239:213–248, 1992.